

Multi-scale Dynamics of Organic Light-Emitting Devices

A dissertation submitted to the faculty of the graduate school of the University of
Minnesota

Kyle William Hershey

In partial fulfillment of the requirements for the degree of Doctor of Philosophy

Russell J. Holmes, Advisor

January 4, 2018

Acknowledgements

I would like to thank my research advisor Russell J. Holmes for all of his guidance and advice.

Parents

Mary Beth

Dow Chemical for funding and collaboration. Dow scientists for research guidance, samples, etc.

Dedication

To some people that I value

Abstract

Over the last decade, organic light-emitting devices (OLEDs) have grown to receive tremendous attention for application in commercial displays and in lighting. While mostly successful for small format displays, challenges still exist that limit their performance for broader applications. Many of these limitations stem from a lack of understanding of charge and exciton dynamics and their impact on efficiency and stability. In this presentation, we describe novel device characterization and modelling efforts aimed at elucidating key dynamic processes in multiple regimes, including the microsecond transient behavior, steady-state, and long term degradation.

A model is presented which unifies both the transient and steady-state electroluminescence behavior of an OLED as a function of current density. The excellent agreement between the model and experiment enables a deeper understanding of efficiency reduction at high brightness. Additionally, the relatively ambiguous device efficiency parameter of charge balance is recast as an exciton formation efficiency. This framework permits a novel characterization paradigm for decoupling degradation pathways during OLED life-testing. In addition to the luminance loss, the degradation in emitter photoluminescence and exciton formation efficiency are also extracted. This technique is applied to an archetypical phosphorescent OLEDs, enabling more comprehensive design rules for device engineering to realize enhanced lifetime. Data science is a rising topic in industrial research. A system for enabling data science techniques within laboratory research is presented. Select useful applications are demonstrated.

Contents

1	Overview of Organic Semiconductors	4
1.1	Organic Semiconductors	4
1.2	Excitons	4
1.2.1	Singlets and Triplets	4
1.2.2	Electronic Transitions	4
1.3	Charge Transport	4
2	Organic Light-Emitting Devices	5
2.1	Fabrication Processes	6
2.2	Characterization	6
2.2.1	Luminance	6
2.2.2	Efficiency Analysis	6
2.3	Historical Development	6
2.3.1	The First OLEDs	6
2.3.2	Phosphorescence	6
2.3.3	Host-Guest Systems	6
2.3.4	Cohost Systems	6
2.3.5	Thermally Activated Delayed Fluorescence	6
2.4	Device Operation	6
2.4.1	Dynamic Processes	6
2.4.2	Efficiency Roll-Off	6
2.5	Recombination Zone Characterization	6
2.6	Single Carrier Devices	6
3	Transient and Steady-State Dynamics	7
3.1	Motivation	7
3.2	Theory	8
3.2.1	Exciton Dynamics	8
3.3	Polaron Dynamics	10
3.4	Exciton Quenching in Photoluminescence	11
3.4.1	Transient Electroluminescence	11
3.4.2	Efficiency Analysis	11
3.5	Experimental Details	13
3.6	Application to Devices	13
3.6.1	Overview of Approach	13
3.6.2	Initializing Parameters with Quenching Only Steady-State Model	13
3.6.3	Transient Modeling	13
3.6.4	Term Efficiency During Transient	13
3.6.5	Extracting Exciton Formation Efficiency	13
3.6.6	Drift Model	13
3.7	Understanding Assumptions of Polaron Model	14
3.7.1	Carrier Injection	14

3.7.2	Charge Imbalance	15
4	Integrated Photoluminescence Lifetimes	17
4.1	Luminance as Efficiency Loss	17
4.2	Photoluminescence Characterization	17
4.2.1	Light Selection	18
4.2.2	Absorption - Recombination Overlap	18
4.2.3	Contact Degradation	18
4.2.4	Quenching Changes During Degradation	18
4.2.5	Verification with Excton Lifetime	18
4.3	Experimental Implementation	18
4.3.1	Hardware Setup	18
4.3.2	Software Developement	18
4.3.3	Database Integration	18
5	Applied Integrated Lifetimes	21
5.1	CBP Host Thickness	21
5.2	MEML Luminance Scaling	21
5.3	Dow Cohost	21
6	Novel Blue Emitter Developement	24
6.1	Molecular Systems	24
6.2	Performance Optimization	24
6.3	Solution Molecular Aggregation	24
7	Data Management for Devices	25
8	Modeling Out-Coupling	26
8.1	Theory	26
8.2	Recombination Zone Overlap During Lifetime	26
9	Future Research	27
	Bibliography	27
	Appendices	33
A	List of Publications	33
A.1	Measuring Triplet Energies	33
B	Out-Coupling Code	34
C	Lifetime Box Code	35
	List of Figures	35
	List of Tables	38

Chapter 1

Overview of Organic Semiconductors

1.1 Organic Semiconductors

1.2 Excitons

1.2.1 Singlets and Triplets

1.2.2 Electronic Transitions

1.3 Charge Transport

Chapter 2

Organic Light-Emitting Devices

2.1 Fabrication Processes

2.2 Characterization

2.2.1 Luminance

2.2.2 Efficiency Analysis

2.3 Historical Developement

2.3.1 The First OLEDs

2.3.2 Phosphorescence

2.3.3 Host-Guest Systems

2.3.4 Cohost Systems

2.3.5 Thermally Activated Delayed Fluorescence

2.4 Device Operation

2.4.1 Dynamic Processes

2.4.2 Efficiency Roll-Off

2.5 Recombination Zone Characterization

2.6 Single Carrier Devices

Chapter 3

Transient and Steady-State Dynamics

This section is an extension of my previous work entitled “*Unified analysis of transient and steady-state electrophosphorescence using exciton and polaron dynamics modeling*”. [11]

3.1 Motivation

As discussed in Chapter 2, modern OLEDs are typically based around Phosphorescent emitters in order to realize 100% internal efficiencies.[4, 3, 30, 19] However, these phosphorescent emitters, while allowing emission out of the triplet excitonic state, also suffer from the drawback of a longer exciton lifetime, typically on the order of 10^{-6} - 10^{-3} s.[3, 13] An increased lifetime leads to a larger steady-state triplet exciton density compared to a fluorescent device operating at the same luminance. This becomes problematic at the high current densities associated with high brightness due to well documented quenching events.[24, 23, 22, 17, 14, 28, 6] These quenching events lead to a reduced quantum efficiency at high-current, and termed the “Efficiency roll-off”.

Efficiency roll-off is well attributed to quenching and is ubiquitous to phosphorescent OLED behavior.[24, 6, 18, 7] While previous works have attributed the roll-off to quenching, they have failed to provide a complete picture of the exciton and charge dynamics within the device. All of these works have utilized a differential equations model for the exciton dynamics, solved in the steady state. This becomes apparent when investigating the transient electroluminescence (EL), where a transient voltage pulse, on the order of 500 ns is applied to the device and the resulting luminance is recorded as a function of time. Figure 3.1 is an attempt to fit the transient luminance decay using the model presented by Reineke *et al.* which well fits the efficiency roll-off. Indeed, this is a well known problem with existing models, and previous attempts to model the transient EL have utilized an empirical biexponential function to quantify the decay.[6, 7, 2, 33]

In addition to failing to replicate the luminance decay, no known previous efforts have been made in trying to replicate the experimental transient EL luminance rise.

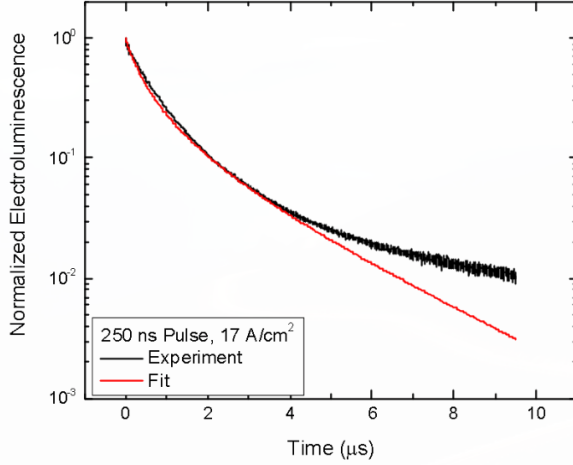


Figure 3.1: Fitting the transient electroluminescence decay without polaron dynamics.

In addition to the problems with the transient electroluminescence, the interpretation of the existing model without a full dynamics picture can lead to false predictions. Figure 3.2a shows what a quenching model predicts for the roll-off as a function of increasing recombination zone width. However, even in the most idealized case of a gradient emissive layer device, where no additional interfaces come into play, the predictive model fails to replicate the behavior, as shown in Figure 3.2b. While this device is of little interest for further investigation due to the extreme thickness, the point stands that this model has glaring assumptions for its applications.

Both the transient EL and the recombination zone dependence issues arise due to an incomplete picture of the device physics, more specifically in the area of polaron dynamics. This work sought to address these issues by including polaron dynamics. Since the steady-state solution of existing models is able to accurately replicate steady-state performance, the transient EL is utilized as well as the steady-state solution to ensure that the underlying physics are accurately captured. A valid solution should be able to accurately fit both regimes using the same model parameter values. In order to leverage previous work, the archetypical green-emitter tris[2-phenylpyridinato-c₂,N]Iridium(III) (Ir(ppy)₃) is used for the extensively characterized photophysics.[4, 2, 29, 1, 15, 16]

3.2 Theory

3.2.1 Exciton Dynamics

The dominant processes that influence the exciton population, first formalized by Reineke *et al.*[24], have been identified as natural exciton decay, via radiative and non-radiative processes, triplet-triplet annihilation, triplet-polaron quenching, and exciton generation.[6, 28] In triplet-triplet annihilation, two triplets are able to interact, and one exciton transfers its energy to the other, resulting in one molecule relaxing to the ground state and the other forming a hot excited state. This hot state releases this additional energy to heat and typically relaxes back to the T_1 state. Triplet-polaron quenching is the interaction of a polaron with a nearby triplet exciton. Here, one of the charges of the exciton non-radiatively recombines with the polaron of the opposite charge, leaving a remaining loose charge. Excitons are also subject to field dissociation, but this mechanism is ignored in this work. Field dissociation is typically observed for fields larger than 2.5×10^6 V/cm. This is near the maximum field used for this study, and would be important to consider for higher voltage characterization.

In agreement with previous models, singlet-triplet exciton intersystem crossing and host-guest exciton energy transfer are assumed to be fast compared to exciton decay.[24, 2, 31] Since these mechanisms are much faster, they will not be rate-limiting processes and can thus be omitted from the differential equations model without sacrificing accuracy. Within an operational device, electron and hole populations are indistinguishable. Therefore, the electron (n_e) and hole (n_h) densities are treated as a single generalized polaron population, $n_{pol} = n_e + n_h$. For simplicity, the model developed here treats the exciton and polaron populations as spatially uniform and confined to the exciton recombination zone. An spatial inhomogeneity in exciton and polaron density as well as their overlap is absorbed into the bimolecular rate constants. It is important to note that due to this assumption, rate constants are a property of the device stack, and not just a material property. With these assumptions, the dynamic processes determining exciton density (n_{ex}) can be summarized in the following one-dimensional rate equation:

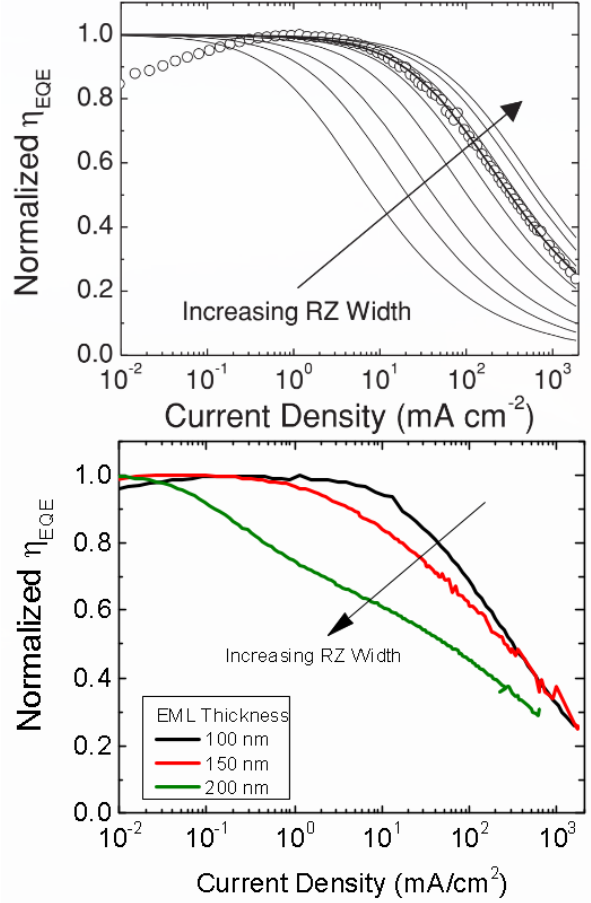


Figure 3.2: (a) Efficiency roll-off predicted by Erickson *et al.* 2014 as a function of recombination zone width. (b) Observed efficiency roll-off for gradient EML devices.

$$\frac{dn_{ex}}{dt} = -\frac{n_{ex}}{\tau} - \frac{1}{2}k_{TT}n_{ex}^2 - k_{TP}n_{pol}n_{ex} + G_{ex} \quad (3.1)$$

where τ is the natural exciton lifetime, determined by the radiative (k_r) and non-radiative (k_{nr}) decay rates by $\tau = 1/(k_r + k_{nr})$, k_{TT} is the rate constant for triplet-triplet annihilation, k_{TP} is the rate constant for triplet-polaron quenching, and G_{ex} is the exciton generation rate. As this is a one-dimensional model, G_{ex} is a spatially uniform generation rate, a simplifying assumption. Many studies have modeled the exciton recombination zone profile, relying on material energy levels, as well as mobilities.[25, 8, 9, 26, 27] While these models are more accurate and explicit, in the way that they capture the physics, they also increase the dimensionality of our model, as well as increasing the parameterization; requiring separate electron and hole rate equations, mobilities and energy levels for every material. Even with this increased accuracy of the physical processes, identifying if the predicted exciton recombination zone is accurate requires significant additional measurements. Since the goal of this work is to provide a functional model to accurately predict the transient and steady-state device behavior, spatially uniform dynamics are assumed. Here, exciton formation is treated using a Langevin recombination formalism based on the polaron density.[26, 20, 5]

$$G_{ex} = \frac{k_F}{4}n_{pol}^2 \quad (3.2)$$

where k_F is the rate constant for exciton formation. The factor of four accounts for the diversity of the polaron population and assumes that electrons and holes are in equal proportion. The accuracy of this prefactor is reduced for imbalanced charge, and is investigated in Section 3.7.2. For $n_e:n_h$ ratios 2:1 or better, less than 20% error is found in this term.

3.3 Polaron Dynamics

Previous models for efficiency roll-off have ignored polaron dynamics and assumed that all polarons readily form excitons. The steady-state polaron density is then modeled using a space charge limited model.[21] To attribute physics to this process, a simple picture of polaron dynamics is assumed, consisting of charge injection and transport, exciton formation, and polaron loss. In order to preserve our one-dimensionality, polarons must be uniformly distributed. Without competing losses in the transport layers, all injected polarons must eventually reach the emissive layer. We further assume that polarons easily enter that emissive layer and that the majority of polaron build up occurs within the emissive layer, rather than the transport layers. Therefore, the charges injected from the current density, J , are uniformly generated in the emissive layer by $G_{pol} = 2J/ew$. Here, e is the electron charge, and the factor of two arises from an assumption of equal

charge injection. In a well balanced device, the measured current forms holes on one side of the device and electrons on the other, and are both injected into the device. This is discussed extensively in Section 3.7.1. Polaron losses to exciton formation mirror the exciton formation rate presented in Equation 3.2, though at twice the rate due to two polarons forming one exciton.

The introduction of polaron loss from the emissive layer through the device without forming excitons is essential to address the limitations of previous models. Without this term, peak internal quantum efficiency of all devices is assumed to be 100% and the roll-up of efficiency at low current can not be explained. In order to capture polaron loss, a first order approximation is made for loss in that only the majority charge carrier can be lost and leaks through the device with a characteristic time, τ_l . With these mechanisms, the full polaron dynamics can be expressed as:

$$\frac{dn_{pol}}{dt} = \frac{-k_F}{2} n_{pol}^2 - \frac{n_{pol}}{\tau_l} + G_{pol}. \quad (3.3)$$

3.4 Exciton Quenching in Photoluminescence

$$V = \left[\frac{J}{e\mu N_C} d^{2l+} \left(\frac{eN_0 k_B T_t}{\epsilon} \right)^l \right]^{\frac{1}{l+1}} = C J^{\frac{1}{l+1}} \quad (3.4)$$

$$n_{pol} = eN_c \left(\frac{\epsilon V}{ed^2 N_0 k_B T_t} \right)^l \quad (3.5)$$

$$\frac{L(n_{pol})}{L_0} = \frac{1}{1 + \tau k_{TP} n_{pol}} \quad (3.6)$$

3.4.1 Transient Electroluminescence

3.4.2 Efficiency Analysis

$$\eta_{EQE} = \eta_{OC} \eta_{PL} \chi \eta_{EF} \quad (3.7)$$

$$\eta_{EQE} = \frac{\eta_{OC} \eta_{ex} k_r}{G_{pol}/2} \quad (3.8)$$

$$\eta_{EF} = \frac{\frac{1}{2} k_F n_{pol}}{G_{pol}} = \frac{\frac{1}{2} k_F n_{pol}}{\frac{1}{2} k_F n_{pol} + \frac{1}{\tau_l}} \quad (3.9)$$

3.5 Experimental Details

3.6 Application to Devices

3.6.1 Overview of Approach

3.6.2 Initializing Parameters with Quenching Only Steady-State Model

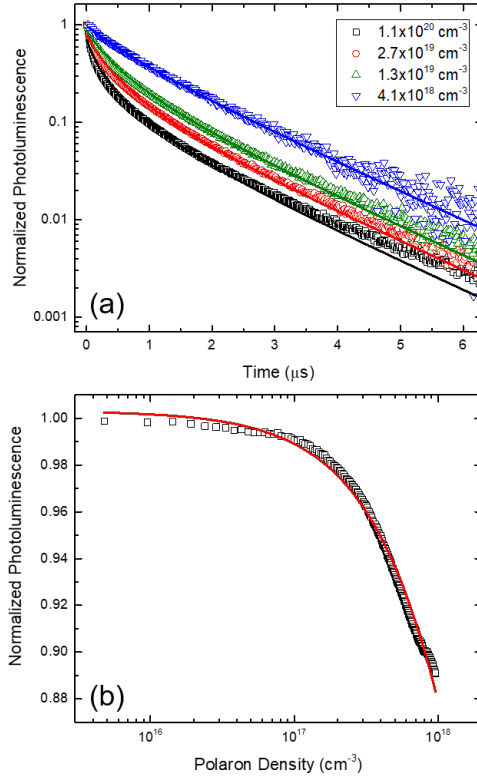
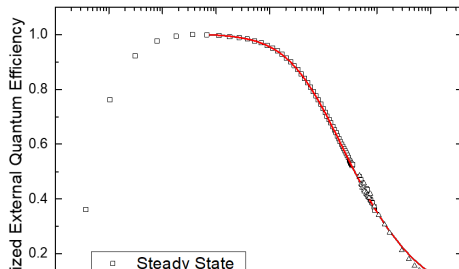


Figure 3.3: (a) Transient photoluminescence (PL) decays for several initial exciton densities with fits shown as solid lines using Eqn. 3.2. Fit parameters are discussed in SECTION. Exciton densities are calculated using measured incident power and beam size in combination with Beer's Law. (b) Steady-state PL quenching as a function of polaron density and the resulting fit from Eqn. 3.6 shown as the solid line.

3.6.3 Transient Modeling



	Transient EL	Efficiency Roll-off
τ (s)	$6.9 \pm 0.1 \times 10^{-7}$	6.1×10^{-7}
k_{TT} (cm ³ /s)	7.1×10^{-12}	7.1×10^{-12}
k_{TP} (cm ³ /s)	3.3×10^{-13}	3.3×10^{-13}
k_F (cm ³ /s)	$7.7 \pm 3.5 \times 10^{-12}$	1.6×10^{-11}

Table 3.1: Fit parameters extracted from transient and steady-state electroluminescence. Transient EL fit parameters averaged over all measured current densities. η_{EQE} roll-off parameters averaged over several measured devices. Triplet-triplet annihilation and triplet-polaron quenching rates are fixed to those obtained from fitting the normalized efficiency roll-off.

$$\tau_l = \frac{w}{E\mu(E)} \quad (3.10)$$

3.7 Understanding Assumptions of Polaron Model

3.7.1 Carrier Injection

$$\frac{dn_h}{dt} = -k_F n_e n_h - \frac{n_h}{\tau_{lh}} + \frac{J_h}{ew} \quad (3.11)$$

$$\frac{dn_e}{dt} = -k_F n_e n_h - \frac{n_e}{\tau_{le}} + \frac{J_e}{ew} \quad (3.12)$$

$$J_1 \rightarrow J_h = J_2 \rightarrow J_e \quad (3.13)$$

$$\frac{J_e}{ew} + \frac{J_h}{ew} = \frac{J_1 + J_2}{ew} = \frac{2J}{ew} \quad (3.14)$$

$$J_1 = J_h \quad (3.15)$$

$$J_2 = J_e + J_l \quad (3.16)$$

$$J = J_h = J_e + J_l \quad (3.17)$$

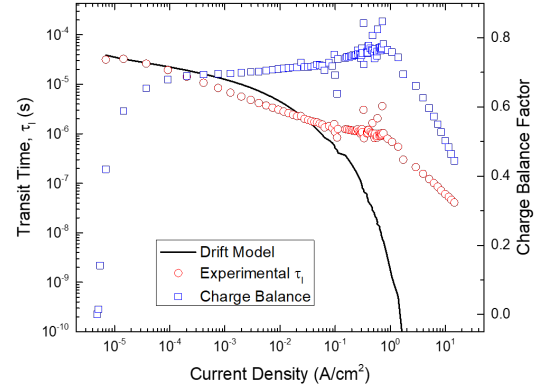


Figure 3.7: Transit time extracted from η_{EQE} measurements are shown as the red circles. Predictions using the drift model are calculated using Eqn. 3.10. The drift model assumes a uniform electric field. Good agreement between the experimental transit time and the drift model is found for a field distributed over 20 nm. The charge balance factor is shown as a function of current density in blue squares.

$$G_{pol} - \frac{J_l}{ew} = \frac{2J - J_l}{ew} \quad (3.18)$$

3.7.2 Charge Imbalance

$$\alpha = \frac{n_h}{n_e + n_h} \quad (3.19)$$

$$\left[\frac{dn_{pol}}{dt} \right]_{formation} = -2k_F n_{pol}^2 \alpha (1 - \alpha) \quad (3.20)$$

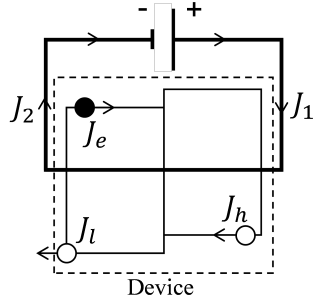


Figure 3.8: Current density formalism within the circuit. J_1 and J_2 are the currents measured on either side of the device. J_e and J_h are the electron and hole currents within the device and J_l is the unbalanced current, assumed to be only holes, that leaks out of the opposing contact.

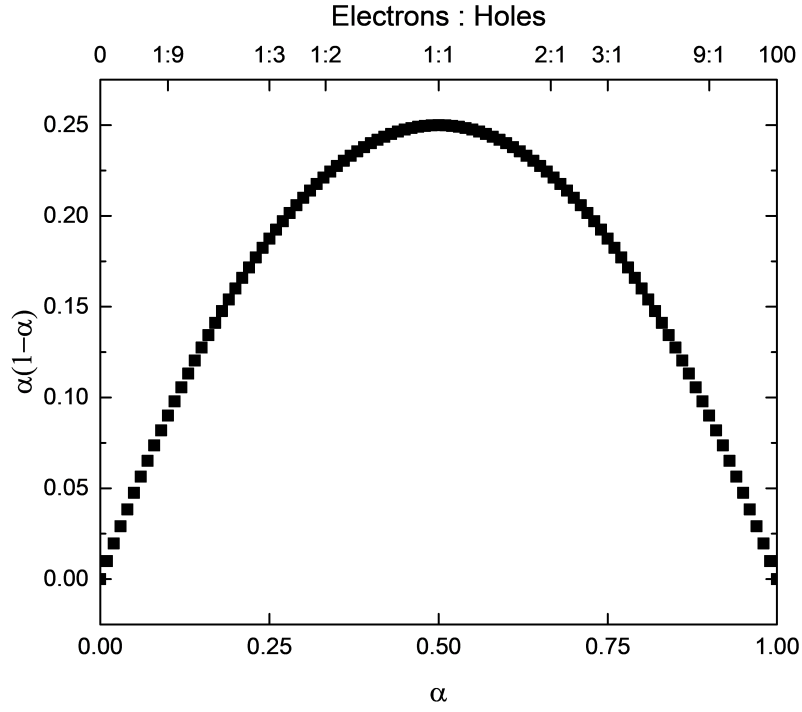


Figure 3.9: The quantity $\alpha(1-\alpha)$ is plotted as a function of the polaron composition, α and the electron to hole ratio.

Chapter 4

Integrated Photoluminescence Lifetimes

4.1 Luminance as Efficiency Loss

$$\eta_{EQE} = \eta_{PL}\eta_{OC}\chi\eta_{EF}\eta_{\tau} \quad (4.1)$$

$$\frac{\eta_{EQE}(t)}{\eta_{EQE}^0} = \frac{\eta_{PL}(t)}{\eta_{PL}^0} \frac{\eta_{EF}(t)}{\eta_{EF}^0} \quad (4.2)$$

4.2 Photoluminescence Characterization

$$\frac{\eta_{PL}(t)}{\eta_{PL}^0} = \frac{L_{PL}(t)}{L_{PL}^0} \frac{I^0}{I(t)} \quad (4.3)$$

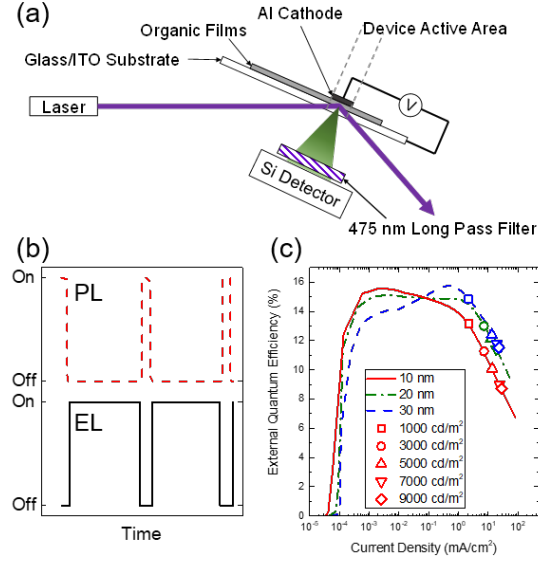


Figure 4.1: (a) Experimental configuration for the measurement of electro- (EL) and photoluminescence (PL) during OLED degradation. Laser excitation is incident on a subsection of the device area. The laser is aligned so that neither the incident nor reflected beam strikes the detector. Stray laser light is removed by a $\lambda=475$ nm dielectric long pass filter. (b) Excitation scheme. EL and PL signals are probed independently with no temporal overlap. (c) External quantum efficiency versus current density and luminance for devices having emissive layer thickness of 10 nm, 20 nm and 30 nm.

4.2.1 Light Selection

4.2.2 Absorption - Recombination Overlap

4.2.3 Contact Degradation

4.2.4 Quenching Changes During Degradation

4.2.5 Verification with Excton Lifetime

4.3 Experimental Implementation

4.3.1 Hardware Setup

4.3.2 Software Developement

4.3.3 Database Integration

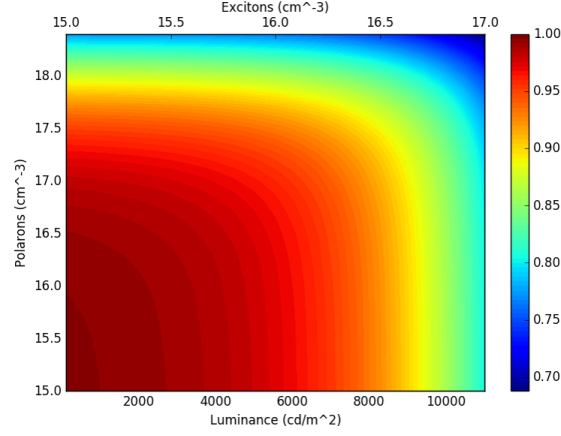


Figure 4.2: Multiplicative correction factor for exciton formation efficiency due to changes in quenching during lifetime. Shown as a function of polaron and exciton density as well as luminance, assuming a 10 nm emissive layer.

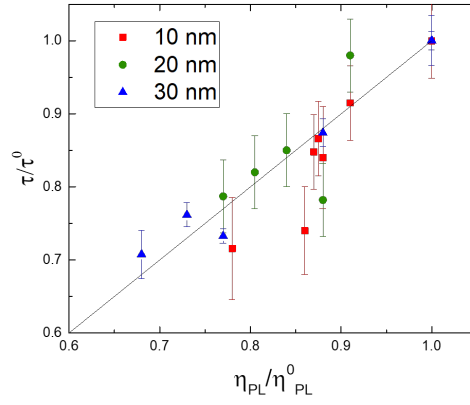


Figure 4.3: Exciton lifetime ratio extracted from transient PL measurements on degraded and undegraded devices as a function of emissive layer thickness.

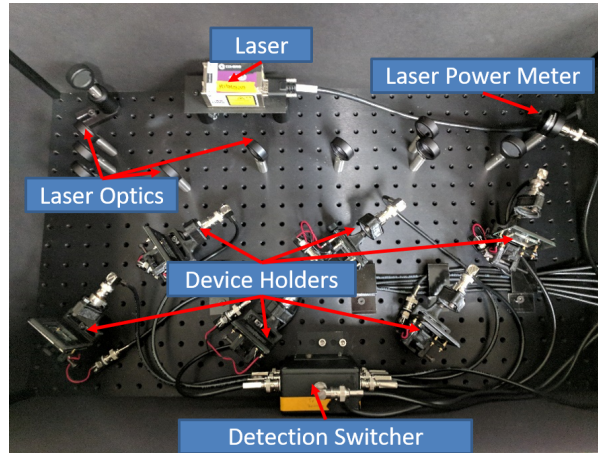


Figure 4.4: Device contacting, measurement, and optical hardware. Version 3 of the hardware is shown. Controlling hardware is shown in Fig. 4.5

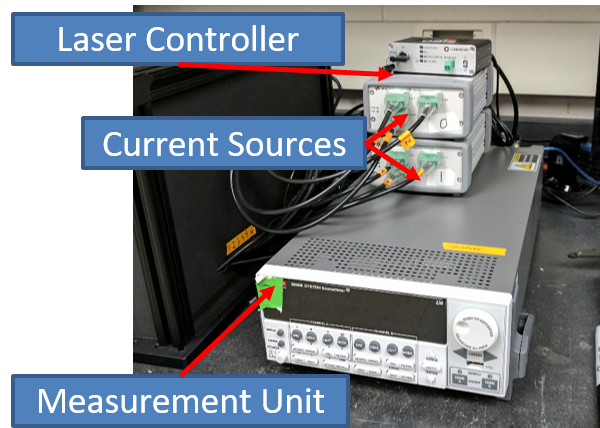


Figure 4.5: Source-Measure hardware and laser controller

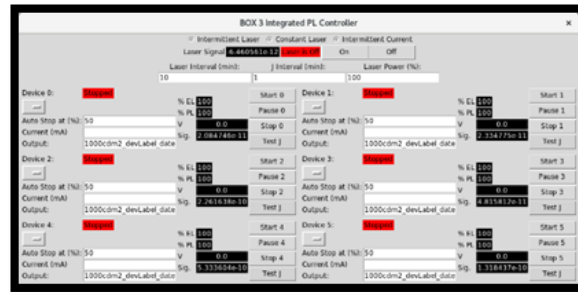


Figure 4.6: 6 channel software controller. Selection of test type, laser control for alignment, and global settings are accessible on the top of the interface. Individual channel settings are grouped on the bottom.

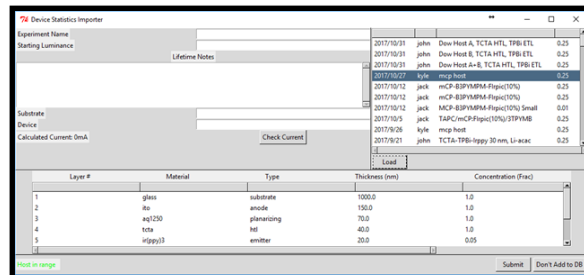


Figure 4.7: Test information for database import interface. The top left panel collects information about the specific device and lifetime. The right panel connects the device to a particular growth and architecture. The bottom panel confirms the architecture.

Chapter 5

Applied Integrated Lifetimes

5.1 CBP Host Thickness

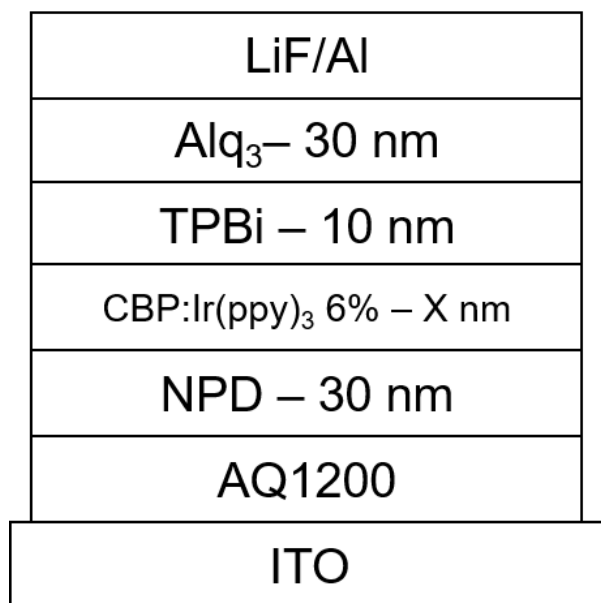


Figure 5.1: Device architecture, featuring EML thicknesses of X=10,20, and 30 nm

5.2 MEML Luminance Scaling

5.3 Dow Cohost

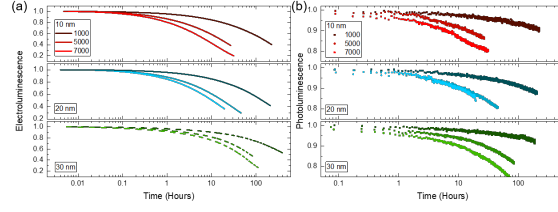


Figure 5.2: Device decay curves for multiple values of the initial luminance as a function of emissive layer thickness. Loss in (a) electroluminescence (EL) and (b) photoluminescence (PL) are shown and decrease monotonically with increasing luminance. For devices with a 10-nm-thick emissive layer, initial luminance values are 1000 cd/m^2 , 5000 cd/m^2 , and 7000 cd/m^2 . For devices with a 20-nm- or 30-nm-thick emissive layer, initial luminance values are 1000 cd/m^2 , 5000 cd/m^2 , and 7100 cd/m^2 .

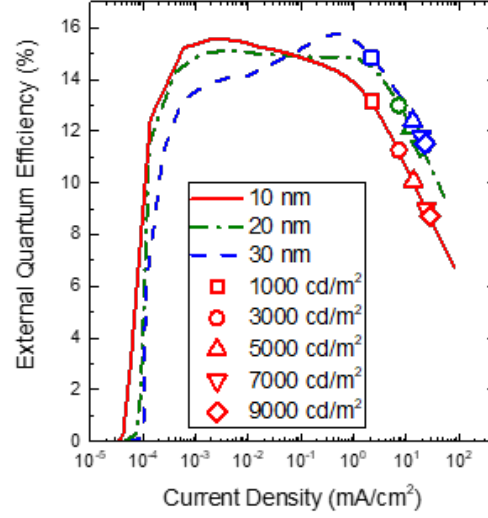


Figure 5.3: External Quantum Efficiency (η_{EQE}) for the three architectures. Operational points for lifetime are shown in symbols.

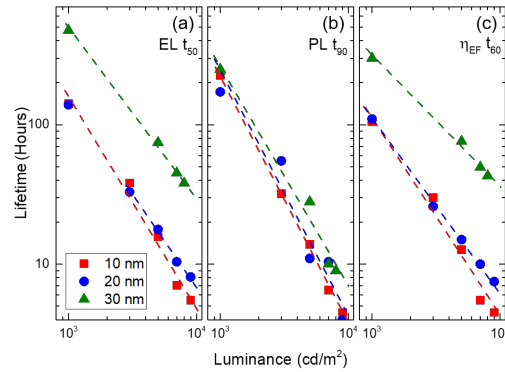


Figure 5.4: Extracted lifetimes for all 3 architectures as a function of luminance.

d_{EML} (nm)	L_0 (cd/m ²)	J (mA/cm ²)	V_0 (V)	t_{50} (hours)
10	1000	2.2	4.2	139.0
	3000	7.2	5.1	39.9
	5000	13.6	5.4	15.8
	7000	14.4	6.2	6.9
	9000	28.0	6.3	5.3
20	1000	2.2	5.4	141.1
	3000	7.2	6.0	33.1
	5000	12.4	7.2	17.2
	7100	19.2	7.3	10.0
	9000	24.0	7.5	8.0
30	1000	2.2	5.9	474
	5000	13.6	7.3	74.4
	7100	19.6	7.6	46
	8000	22.4	7.7	38.1

Table 5.1: Summary of device lifetimes. For each device, the starting luminance (L_0), current density (J), starting voltage (V_0) and time at which 50% of the initial luminance is reached (t_{50}) are reported.

Chapter 6

Novel Blue Emitter Developement

6.1 Molecular Systems

6.2 Performance Optimization

6.3 Solution Molecular Aggregation

Chapter 7

Data Management for Devices

Chapter 8

Modeling Out-Coupling

8.1 Theory

8.2 Recombination Zone Overlap During Lifetime

Chapter 9

Future Research

Bibliography

- [1] ADACHI, C., KWONG, R., AND FORREST, S. R. Efficient electrophosphorescence using a doped ambipolar conductive molecular organic thin film. *Organic Electronics* 2, 1 (mar 2001), 37–43.
- [2] BALDO, M., ADACHI, C., AND FORREST, S. R. Transient analysis of organic electrophosphorescence. II. Transient analysis of triplet-triplet annihilation. *Physical Review B* 62, 16 (oct 2000), 10967–10977.
- [3] BALDO, M., O'BRIEN, D., YOU, Y., SHOUSTIKOV, A., SIBLEY, S., THOMPSON, M. E., AND FORREST, S. R. Highly efficient phosphorescent emission from organic electroluminescent devices. *Nature* 395, September (1998), 151–154.
- [4] BALDO, M., THOMPSON, M. E., AND FORREST, S. High-efficiency fluorescent organic light-emitting devices using a phosphorescent sensitizer. *Nature* 403, 6771 (feb 2000), 750–3.
- [5] BLOM, P. W. M., DE JONG, M. J. M., AND VLEGGAAR, J. J. M. Electron and hole transport in poly(p-phenylene vinylene) devices. *Applied Physics Letters* 68, 23 (1996), 3308–3310.
- [6] ERICKSON, N. C., AND HOLMES, R. J. Engineering efficiency roll-off in organic light-emitting devices. *Advanced Functional Materials* 24 (2014), 6074–6080.
- [7] GIEBINK, N. C., AND FORREST, S. R. Quantum efficiency roll-off at high brightness in fluorescent and phosphorescent organic light emitting diodes. *Physical Review B* 77, 23 (jun 2008), 235215.
- [8] HASSINE, L., BOUCHRIHA, H., ROUSSEL, J., AND FAVE, J. L. Transient response of a bilayer organic electroluminescent diode: Experimental and theoretical study of electroluminescence onset. *Applied Physics Letters* 78, 8 (2001), 1053–1055.
- [9] HASSINE, L., BOUCHRIHA, H., ROUSSEL, J., AND FAVE, J. L. Transient response of a bilayer organic light emitting diode: Building-up of external and recombination currents. *Journal of Applied Physics* 91, 8 (2002), 5170–5175.

- [10] HERSHEY, K. W., AND COTTINGHAM, J. P. Material properties of pipes and reeds from the Southeast Asian khaen. *The Journal of the Acoustical Society of America* 129, 4 (apr 2011), 2520–2520.
- [11] HERSHEY, K. W., AND HOLMES, R. J. Unified analysis of transient and steady-state electrophosphorescence using exciton and polaron dynamics modeling. *Journal of Applied Physics* 120, 19 (2016), 195501.
- [12] HERSHEY, K. W., SUDDARD-BANGSUND, J., QIAN, G., AND HOLMES, R. J. Decoupling degradation in exciton formation and recombination during lifetime testing of organic light-emitting devices. *Applied Physics Letters* 111, 11 (2017), 113301.
- [13] HOLMES, R. J., FORREST, S. R., TUNG, Y.-J., KWONG, R. C., BROWN, J. J., GARON, S., AND THOMPSON, M. E. Blue organic electrophosphorescence using exothermic hostguest energy transfer. *Applied Physics Letters* 82, 15 (2003), 2422.
- [14] KALINOWSKI, J., STAMPOR, W., MŻYK, J., COCCHI, M., VIRGILI, D., FATTORI, V., AND DI MARCO, P. Quenching effects in organic electrophosphorescence. *Physical Review B* 66, 23 (dec 2002), 235321.
- [15] KAWAMURA, Y., BROOKS, J., BROWN, J. J., SASABE, H., AND ADACHI, C. Intermolecular interaction and a concentration-Quenching mechanism of phosphorescent Ir(III) complexes in a solid film. *Physical Review Letters* 96, 1 (2006), 11–14.
- [16] KAWAMURA, Y., GOUSHI, K., BROOKS, J., BROWN, J. J., SASABE, H., AND ADACHI, C. 100% phosphorescence quantum efficiency of Ir (III) complexes in organic semiconductor films. *Applied Physics Letters* 86, 7 (2005), 1–3.
- [17] MEZYK, J., KALINOWSKI, J., MEINARDI, F., AND TUBINO, R. Triplet exciton interactions in solid films of an electrophosphorescent Pt (II) porphyrin. *Applied Physics Letters* 86, 11 (2005), 111916.
- [18] MURAWSKI, C., LEO, K., AND GATHER, M. C. Efficiency roll-off in organic light-emitting diodes. *Advanced materials (Deerfield Beach, Fla.)* 25, 47 (dec 2013), 6801–27.
- [19] O'BRIEN, D. F., BALDO, M., THOMPSON, M. E., AND FORREST, S. R. Improved energy transfer in electrophosphorescent devices. *Applied Physics Letters* 74, 3 (1999), 442.
- [20] PINNER, D. J., FRIEND, R. H., AND TESSLER, N. Transient electroluminescence of polymer light emitting diodes using electrical pulses. *Journal of Applied Physics* 86, 9 (1999), 5116–5130.
- [21] POPE, M., AND SWENBERG, C. *Electronic Processes in Organic Crystals and Polymers*, 2nd ed. Oxford University Press, 1999.

- [22] REINEKE, S., SCHWARTZ, G., WALZER, K., FALKE, M., AND LEO, K. Highly phosphorescent organic mixed films: The effect of aggregation on triplet-triplet annihilation. *Applied Physics Letters* 94, 16 (2009), 2007–2010.
- [23] REINEKE, S., SCHWARTZ, G., WALZER, K., AND LEO, K. Reduced efficiency roll-off in phosphorescent organic light emitting diodes by suppression of triplet-triplet annihilation. *Applied Physics Letters* 91, 12 (2007), 1–4.
- [24] REINEKE, S., WALZER, K., AND LEO, K. Triplet-exciton quenching in organic phosphorescent light-emitting diodes with Ir-based emitters. *Physical Review B* 75, 12 (mar 2007), 125328.
- [25] RIHANI, A., HASSINE, L., FAVE, J.-L., AND BOUCHRIHA, H. Study of the transient EL slow rise in single layer OLEDs. *Organic Electronics* 7, 1 (feb 2006), 1–7.
- [26] RUHSTALLER, B., BEIERLEIN, T., RIEL, H., KARG, S., SCOTT, J., AND RIESS, W. Simulating electronic and optical processes in multilayer organic light-emitting devices. *IEEE Journal of Selected Topics in Quantum Electronics* 9, 3 (2003), 723–731.
- [27] RUHSTALLER, B., CARTER, S. A., BARTH, S., RIEL, H., RIESS, W., AND SCOTT, J. C. Transient and steady-state behavior of space charges in multilayer organic light-emitting diodes. *Journal of Applied Physics* 89, 8 (2001), 4575–4586.
- [28] SONG, D., ZHAO, S., LUO, Y., AND AZIZ, H. Causes of efficiency roll-off in phosphorescent organic light emitting devices: Triplet-triplet annihilation versus triplet-polaron quenching. *Applied Physics Letters* 97, 24 (2010), 243304.
- [29] TSUBOI, T., MURAYAMA, H., AND PENZKOFER, A. Photoluminescence characteristics of Ir(ppy)₃ and PtOEP doped in TPD host material. *Thin Solid Films* 499, 1-2 (2006), 306–312.
- [30] TSUTSUI, T., YANG, M.-J., YAHIRO, M., NAKAMURA, K., WATANABE, T., TSUJI, T., FUKUDA, Y., WAKIMOTO, T., AND MIYAGUTI, S. High Quantum Efficiency in Organic Light-Emitting Devices with Iridium-Complex as a Triplet Emissive Center. *Jpn. J. Appl. Phys. Part 2*: 38, 12 (1999), L1502–L1504.
- [31] TURRO, N., SCAIANO, J., AND RAMAMURTHY, V. *Modern Molecular Photochemistry of Organic Molecules*. University Science Books, 1991.
- [32] XU, F., HERSHEY, K. W., HOLMES, R. J., AND HOYE, T. R. Blue-Emitting Arylalkynyl Naphthalene Derivatives via a Hexadehydro-Diels-Alder Cascade Reaction. *Journal of the American Chemical Society* 138, 39 (oct 2016), 12739–12742.

- [33] ZHANG, B., TAN, G., LAM, C. S., YAO, B., HO, C. L., LIU, L., XIE, Z., WONG, W. Y., DING, J., AND WANG, L. High-efficiency single emissive layer white organic light-emitting diodes based on solution-processed dendritic host and new orange-emitting iridium complex. *Advanced Materials* *24*, 14 (2012), 1873–1877.

Appendices

Appendix A

List of Publications

- HERSHEY, K. W., AND COTTINGHAM, J. P. Material properties of pipes and reeds from the Southeast Asian khaen. *The Journal of the Acoustical Society of America* 129, 4 (apr 2011), 2520–2520
- HERSHEY, K. W., AND HOLMES, R. J. Unified analysis of transient and steady-state electrophosphorescence using exciton and polaron dynamics modeling. *Journal of Applied Physics* 120, 19 (2016), 195501
- HERSHEY, K. W., SUDDARD-BANGSUND, J., QIAN, G., AND HOLMES, R. J. Decoupling degradation in exciton formation and recombination during lifetime testing of organic light-emitting devices. *Applied Physics Letters* 111, 11 (2017), 113301
- XU, F., HERSHEY, K. W., HOLMES, R. J., AND HOYE, T. R. Blue-Emitting Arylalkynyl Naphthalene Derivatives via a Hexadehydro-Diels-Alder Cascade Reaction. *Journal of the American Chemical Society* 138, 39 (oct 2016), 12739–12742

A.1 Measuring Triplet Energies

Appendix B

Out-Coupling Code

Appendix C

Lifetime Box Code

List of Figures

3.1	Fitting the transient electroluminescence decay without polaron dynamics.	8
3.2	(a) Efficiency roll-off predicted by Erickson <i>et al.</i> 2014 as a function of recombination zone width. (b) Observed efficiency roll-off for gradient EML devices.	9
3.3	(a) Transient photoluminescence (PL) decays for several initial exciton densities with fits shown as solid lines using Eqn. 3.2. Fit parameters are discussed in SECTION. Exciton densities are calculated using measured incident power and beam size in combination iwht Beer's Law. (b) Steady-state PL quenching as a function of polaron density and the resulting fit from Eqn. 3.6 shown as the solid line.	13
3.4	Normalized experimental η_{EQE} as a function of current density. Solid line is a fit to the data using Eqn. 3.1 and 3.3 in the absence of polaron loss. Pulsed η_{EQE} measurements are conducted using low duty cycle pulses to steady-state luminance to reduce Joule heating in device.	13
3.5	Transient electroluminescence (EL) for four different current densities (J) and device areas (A). (a) 0.25 cm^2 device at a current density during the pulse of $J = 0.9 \text{ A/cm}^2$ (b) 0.25 cm^2 device at $J = 2.2 \text{ A/cm}^2$ (c) 0.0079 cm^2 device at $J = 7.6 \text{ A/cm}^2$ (d) 0.0079 cm^2 device at $J = 38 \text{ A/cm}^2$	13
3.6	Term efficiency for each dynamical process influencing the exciton population for (a) 0.25 cm^2 device operated at 0.9 A/cm^2 for 500 ns and (b) 0.785 mm^2 device operated at a current density of 38 A/cm^2 for 250 ns. Relative term amplitude is calculated as the magnitude of each term in Eqn. 3.1 divided by the sum of absolute values of each term.	13

3.7	Transit time extracted from η_{EQE} measurements are shown as the red circles. Predictions using the drift model are calculated using Eqn. 3.10. The drift model assumes a uniform electric field. Good agreement between the experimental transit time and the drift model is found for a field distributed over 20 nm. The charge balance factor is shown as a function of current density in blue squares.	14
3.8	Current density formalism within the circuit. and are the currents measured on either side of the device. and are the electron and hole currents within the device and is the unbalanced current, assumed to be only holes, that leaks out of the opposing contact.	15
3.9	The quantity $\alpha(1 - \alpha)$ is plotted as a function of the polaron composition, α and the electron to hole ratio.	16
4.1	(a) Experimental configuration for the measurement of electro- (EL) and photoluminescence (PL) during OLED degradation. Laser excitation is incident on a subsection of the device area. The laser is aligned so that neither the incident nor reflected beam strikes the detector. Stray laser light is removed by a $\lambda=475$ nm dielectric long pass filter. (b) Excitation scheme. EL and PL signals are probed independently with no temporal overlap. (c) External quantum efficiency versus current density and luminance for devices having emissive layer thickness of 10 nm, 20 nm and 30 nm.	18
4.2	Multiplicative correction factor for exciton formation efficiency due to changes in quenching during lifetime. Shown as a function of polaron and exciton density as well as luminance, assuming a 10 nm emissive layer.	19
4.3	Exciton lifetime ratio extracted from transient PL measurements on degraded and undegraded devices as a function of emissive layer thickness.	19
4.4	Device contacting, measurement, and optical hardware. Version 3 of the hardware is shown. Controlling hardware is shown in Fig. 4.5	19
4.5	Source-Measure hardware and laser controller	20
4.6	6 channel software controller. Selection of test type, laser control for alignment, and global settings are accessible on the top of the interface. Individual channel settings are grouped on the bottom.	20
4.7	Test information for database import interface. The top left panel collects information about the specific device and lifetime. The right panel connects the device to a particular growth and architecture. The bottom panel confirms the architecture.	20
5.1	Device architecture, featuring EML thicknesses of X=10,20, and 30 nm	21

5.2	Device decay curves for multiple values of the initial luminance as a function of emissive layer thickness. Loss in (a) electroluminescence (EL) and (b) photoluminescence (PL) are shown and decrease monotonically with increasing luminance. For devices with a 10-nm-thick emissive layer, initial luminance values are 1000 cd/m^2 , 5000 cd/m^2 , and 7000 cd/m^2 . For devices with a 20-nm- or 30-nm-thick emissive layer, initial luminance values are 1000 cd/m^2 , 5000 cd/m^2 , and 7100 cd/m^2	22
5.3	External Quantum Efficiency (η_{EQE}) for the three architectures. Operational points for lifetime are shown in symbols.	22
5.4	Extracted lifetimes for all 3 architectures as a function of luminance.	22

List of Tables

3.1	Fit parameters extracted from transient and steady-state electroluminescence. Transient EL fit parameters averaged over all measured current densities. η_{EQE} roll-off parameters averaged over several measured devices. Triplet-triplet annihilation and triplet-polaron quenching rates are fixed to those obtained from fitting the normalized efficiency roll-off.	14
5.1	Summary of device lifetimes. For each device, the starting luminance (L_0), current density (J), starting voltage (V_0) and time at which 50% of the initial luminance is reached (t_{50}) are reported.	23